JOURNAL OF CATALYSIS 97, 330–343 (1986)

Catalyst Aging Studied with Isotopic Transients: Methanation over Raney Nickel

Y. SOONG, K. KRISHNA, AND P. BILOEN[1]

Department of Chemical and Petroleum Engineering, University of Pittsburgh, Pittsburgh, Pennsylvania 15261

Received May 6, 1985; revised August 26, 1985

Abrupt changes in the reaction ambient from $^{12}CO/H_2$ to $^{13}CO/H_2$ are utilized to obtain transient-kinetic information regarding the causes of activity decline in the methanation over Raney nickel. From the responses we infer that the methanation proceeds via at least two parallel pathways. The relative contribution of the two pathways changes with catalyst aging. The gradual development of a less reactive carbonaceous overlayer alone is insufficient to explain the observations. We conclude that aging affects the nickel catalyst itself. © 1986 Academic Press, Inc.

INTRODUCTION

In order to improve the stability of any heterogeneous catalyst it is necessary to assess the dominant aging mechanism(s). It is desirable to develop tools that discriminate between different aging processes such as: reorganizations in the catalyst adlayer on the one hand (for example, as occurring upon genesis of site-blocking side products), and reorganization of the catalyst itself on the other hand (for example, as occurring upon annealing, facetting or other forms of surface restructuring). The single-most utilized tool for studying catalyst aging is steady-state kinetics; however, steady-state kinetics lacks the ability to discriminate between different aging mechanisms.

To illustrate why steady-state kinetics has limited incisiveness it is useful to focus on a single unidirectional elementary step corresponding to the unimolecular transformation of A* into B*.

For this step, formally denoted by

$$\cdots \rightarrow A^* \xrightarrow{k_A} B^* \rightarrow \cdots$$

we have

$$TOF_B = \frac{\theta_A}{\tau_A} = k_A \theta_A \qquad (1)$$

in which

TOF_B: the rate of formation of B* from A*, expressed per surface-exposed catalyst atom;
θ_A: the abundancy of A*, expressed per surface-exposed catalyst atom;
τ_A: the lifetime of A* (s);
$k_A = \tau_A^{-1}$: the reactivity (constant) of A* (s^{-1}).

At best, steady-state measurements reveal what happens during aging with the *product* $k \cdot \theta$. This is because a TOF (cf. Eq. (1)) is all that is measured. Assessing values for the individual key parameters, k and θ, is beyond the realm of steady-state kinetics (*1, 2*). Accordingly, a site-blocking process primarily affecting θ becomes indistinguishable from a surface-reconstruction process primarily affecting k.

Reactivities (k) and abundancies (θ) of surface intermediates do not correspond in a one-to-one manner with model concepts such as the intrinsic activity and abundancy of active sites (*3*). Therefore, we do *not* want to imply that changes in k and θ upon aging translate necessarily in a one-to-one manner into surface blocking and surface reconstruction. However, k and θ probably

[1] To whom correspondence should be addressed.

0021-9517/86 $3.00

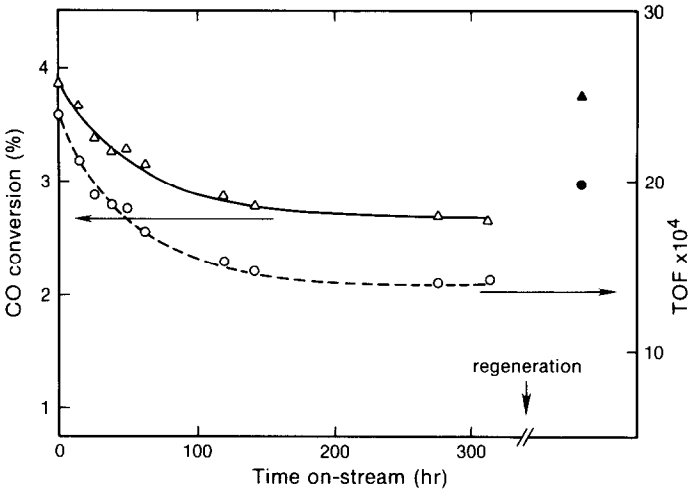

FIG. 1. Effect of aging on conversion (—) and TOF (---). Temperature and SV are kept constant during aging. The lining out time is of the order of 120 h.

are the most fundamental kinetic parameters which we can measure, even though we have to resort to non-steady-state kinetic methods to measure them.

This study reports the behavioral changes of a Raney nickel catalyst during its first 320 h of exposure to hydrogen-lean syngas, as observed with both steady-state and non-steady-state methods. The activity initially declines at a rate of approximately 0.2% per hour, before "lining out" at approximately 68% of its initial value (Fig. 1). This behavior is not unlike that observed in other processes, such as catalytic reforming (*4*). There is recent literature to help assess what is occurring. Methanation proceeds via carbon-derived surface intermediates, CH_x (*5–7, 14*). With prolonged time on stream these species have the tendency to accumulate (*8*), and to deteriorate into a less reactive, hydrogen-poor overlayer (*8–10*). For ruthenium and with hydrogenation in hydrogen-only as the criterion, carbon surface species of distinguishable reactivity are already present after a 300-s exposure to CO/H_2 (*11*). This combined evidence suggests that the following reaction sequence underlies the aging observed in Fig. 1:

$$\begin{array}{ccccccc} CO_{ad} & \xrightarrow{k_a} & CH_x & \xrightarrow{k_b} & CH_y & \xrightarrow{k_c} & \text{C graph.} \\ & & \downarrow k_1 & & \downarrow k_2 & & \\ & & CH_4(g) & & CH_4(g) & & \end{array}$$

SCHEME A

According to Scheme A the synthesis of methane proceeds mainly via "soft carbon," CH_x. This amorphous, hydrogen-rich (*8–10*) surface species tends to deteriorate slowly (k_b), and leads to a slow buildup of less reactive carbon, CH_y. The 120-h line out period is the time needed to balance the CH_y-producing reaction (k_b) by the CH_y-removal reaction (k_2). A very small part of CH_x degrades into "irreactive" carbon, $C_{graphite}$. Very slow building up of this terminal species causes the residual decline after the 120-h lining out period.

Two features are characteristic of the previous interpretation of Fig. 1.

(1) Aging is a process that affects the carbon-derived adlayer rather than the nickel-based catalyst.

(2) The rate of lining out coincides with the rate of attaining a steady-state level of CH_y (Scheme A). Therefore, the experimentally observed lining out time of 120 h (Fig. 1) signals a first-order rate constant, k_2, of the order $k_2 = \frac{1}{120}$ h.

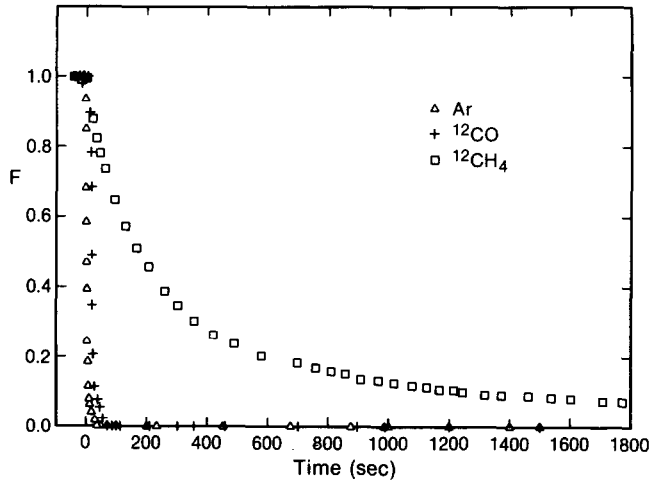

FIG. 2. ^{12}CO and $^{12}CH_4$ transients. The chromatographic separation of Ar and CO allows for the calculation of the amount of CO, adsorbed under steady-state reaction conditions.

During the period represented by Fig. 1 the feed is repeatedly switched from $^{12}CO/H_2$ to $^{13}CO/H_2$. This leads to a transient-kinetic phenomena: the decay of the $^{12}CH_4$ production, which is being compensated by a concurrent increase in the $^{13}CH_4$ production (Fig. 5). As the isotopes ^{12}C and ^{13}C have essentially identical chemical reactivity, these experiments provide transient-kinetic information without disrupting the ongoing surface chemistry. From the changes in the transients accompanying the aging we can obtain (k, θ) information. Although this information does not provide a molecularly detailed picture of the aging process it does lead us to conclude with great certainty that the aging picture discussed in the preceding paragraph and summarized in the Scheme A is essentially *incorrect*.

EXPERIMENTAL

We employed Raney nickel with approximately 10 wt% aluminum. After a 12-h presintering and reduction period in flowing hydrogen (SV = 6000 liters/liter/h) we obtained a BET area around 60 m^2/g and a surface-exposed nickel area, as measured *in situ* with $^{12}CO/^{13}CO$ exchange, around 42 m^2/g. These figures agree with the earlier work of Anderson on low-aluminum Raney nickel (*12*). The nonmetallic part of the surface probably consists predominantly of Al_2O_3 (*12*).

Approximately 0.26 ml of mesh size 60–100 Raney nickel is diluted $\frac{1}{2}$ (v/v) with glass beads and loaded into a $\frac{1}{8}$-in.-i.d. copper-tube reactor. An upstream four-way valve allows abrupt switching from ^{12}CO (Ar-trace) to ^{13}CO, or vice versa. Brooks mass flow controllers and Tescom back-pressure regulators ensure that partial pressures are essentially unaffected by the isotope switch. A trace amount of argon in the ^{12}CO stream serves as an internal time base. At the prevailing SVs (around 1800 liters/liter/h) the rise time of the boundary between phases of different isotopic constitution is approximately 10 s (Fig. 2).

On-line mass spectrometry is performed by continuously sampling the reactor outlet. A small part of the outlet stream is routed via a 0.004-in.-i.d. heated capillary and a Varian flow-by valve into an Extra Nuclear Model 2750-50 quadrupole mass spectrometer. In order to minimize memory effects, the stainless-steel spectrometer housing is permanently heated. This chamber is pumped by a 90-liter/s Leybold–Heraeus turbomolecular pump.

To minimize interference from OH and O

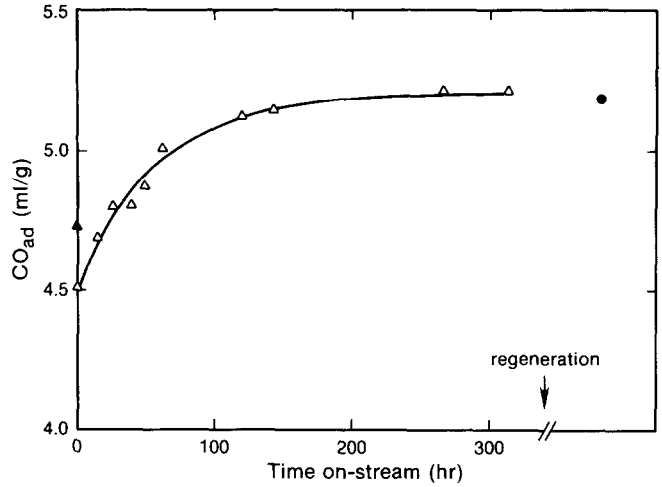

FIG. 3. The effect of aging on the amount of adsorbed CO.

fragments, the open electron-impact ionizer operates at an impact energy of only 20 eV. $^{12}CH_4$ is determined at $m = 15$ and $^{13}CH_4$ at $m = 17$.

RESULTS

After reduction at 400°C for 12 h, the catalyst is cooled down in flowing hydrogen to 110°C. CO is introduced, and the surface-exposed metal area is measured via $^{12}CO/^{13}CO$ exchange (see below). The system is then heated in H_2/CO at a rate of 2°C/min until reaching the reaction temperature (210°C). All times on stream now quoted are taken relatively to the point in time defined by reaching reaction temperature, 210°C.

Within 0.5 h after coming on stream the catalyst reaches maximum activity. The activity initially declines at a rate of approximately 0.2%/h, but lines out after approximately 120 h on stream. The decline after line-out is only approximately 0.7%/24 h (Fig. 1).

When switching off ^{12}CO and Ar simultaneously at the reactor inlet, the production of ^{12}CO at the reactor outlet continues after that of Ar has ceased already (see Fig. 2 for the effect at 210°C). This frontal-elution, chromatographic separation of Ar and ^{12}CO is due to desorption in $^{13}CO/H_2$ atmosphere of an inventory $^{12}CO_{ad}$, which is not paralleled by desorption of a reservoir of Ar_{ad} (*3*, *13*). This effect is routinely used to determine *in situ* the number of surface-exposed nickel atoms. All θ values and TOFs in this paper are obtained by assuming a stoichiometry $CO_{ad}/Ni = 1/1$ for the fresh catalyst at 110°C in a 1-bar atmosphere of $H_2/CO = 10/1$. This assumption is verified by static chemisorption at liquid-nitrogen temperature (*15*).

The chromatographic effect is also observable under reaction conditions (Fig. 2, obtained at $T = 210$°C, $H_2/CO = 2$), and we calculate a CO coverage close to a monolayer. Moreover, the amount of chemisorbed CO increases rather than decreases with time on stream (Fig. 3). In separate measurements we verify that under reaction conditions CO does not chemisorb onto surface carbon. Therefore, we conclude (from Fig. 3) that during aging the surface-exposed metal area increases rather than decreases, probably due to surface roughening accompanying chemicorrosion.

During aging we regularly switch from $^{12}CO/H_2$ to $^{13}CO/H_2$ and vice versa, in order to observe the isotopic transients. We follow and repeat a particular switching pattern (Fig. 4), at 15- to 30-h intervals. A set

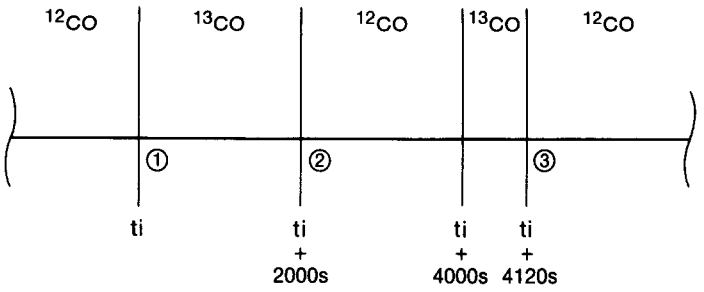

FIG. 4. For a set of times on stream t_i (t_i = 0.5, 16, 40, 64, and 313 h) we followed a switching pattern which produces isotopic transients starting at t_i, t_i + 2000 s, t_i + 4000 s, and t_i + 4120 s.

of transients is shown in Figs. 5–6, and is discussed below.

In response to the switch $^{12}CO/H_2 \rightarrow {}^{13}CO/H_2$ at $t = t_i$ the $^{12}CH_4$ production decreases, and the $^{13}CH_4$ production concurrently increases (Fig. 5). All ordinate values are relative to their respective steady-state values, $F_{12CH_4} = R_{12CH_4}/(R_{12CH_4} + R_{13CH_4})$, etc. It is evident that the transients obey

$$F_{13CH_4} + F_{12CH_4} = 1. \qquad (1a)$$

On close examination the transients starting at $t = t_i$ + 2000 s (Fig. 5) are indistinguishable from those starting at $t = t_i$ (with, of course, $^{12}CH_4$ and $^{13}CH_4$ interchanged). They prove to be indistinguishable also upon curve deconvolution (cf. Discussion). Figure 5 shows four essentially identical transients, provided that we transform the "upcoming" ones (with $dF/dt > 0$) into downcoming ones via the transformation

$$F^* = 1 - F. \qquad (1b)$$

These four transients are averaged, and plotted in Fig. 7 for each different time on stream, t_i. Figure 7 shows one of the main findings of this study, that is, with aging a tail develops in the transients.

The final pair of transients starts at $t = t_i$ + 4120 s, with $^{13}CH_4$ as the downcoming transient. Because prior to the switch to $^{12}CO/H_2$ the catalyst has been exposed to $^{13}CO/H_2$ for only 120 s, $^{13}CH_4$ does start be-

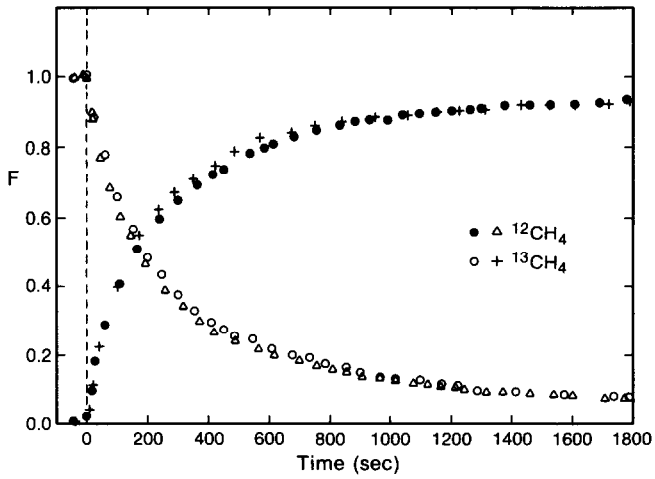

FIG. 5. Normalized methane transients starting at point (1) (Fig. 4); t_i = 25 h, (△) $^{12}CH_4$, (+) $^{13}CH_4$ and starting at point (2) (Fig. 4); t_i = 25 h + 2000 s, (●) $^{12}CH_4$, (○) $^{13}CH_4$.

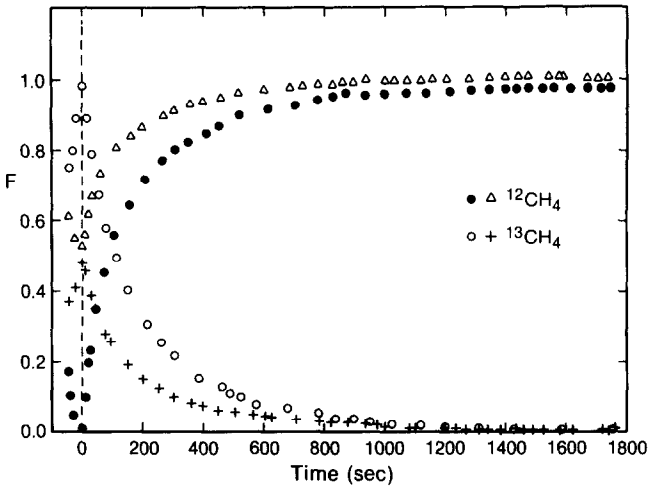

FIG. 6. Methane transients starting at point (3) (Fig. 4); t_i = 25 h + 4120 s, (+) $^{13}CH_4$, (△) $^{12}CH_4$. Because previous exposure to ^{13}CO encompassed only 120 s the starting value of $^{12}CH_4$ is above zero, and that of $^{13}CH_4$ below unity. Normalized transients starting at point (3) (Fig. 4); (○) $^{13}CH_4$, (●) $^{12}CH_4$. Compared to the transients measured at (1) and (2) the tail is lacking ("short exposure changes selectively the content of short-living reservoirs").

low its steady-state value (Fig. 6). In order to allow comparison with the other transients we also normalize the third pair of transients (Fig. 6). This reveals that the normalized $^{13}CH_4$ transient observed after 120 s exposure to ^{13}CO differs from that observed after 2000 s exposure to ^{13}CO. This is another crucial finding. In Fig. 8 we plot the (averaged) transients measured at $t = t_i + 4120$ s (t_i = 0.5 h, 16 h, 40 h, etc.). Unlike the transients measured at $t = t_i$ and $t = t_i + 2000$ s, aging does *not* affect the transients at $t = t_i + 4120$ s.

A few additional experiments will be mentioned in the Discussion section.

DISCUSSION

We start from the observation that the "tails" present in the transients measured at $t = t_i$ and $t = t_i + 2000$ s (cf. Figs. 5 and 6)

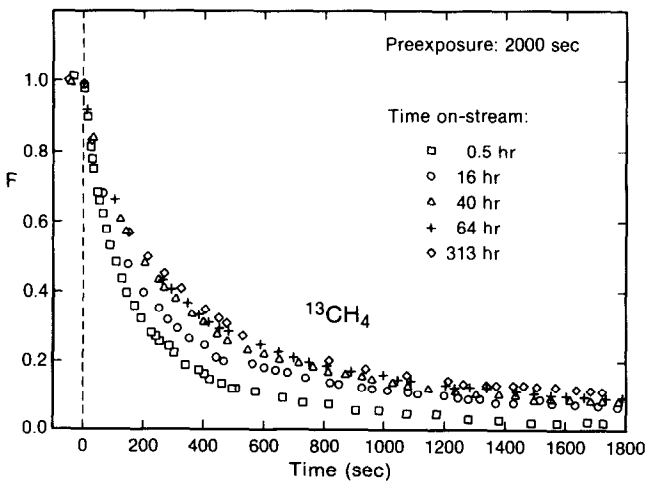

FIG. 7. As a result of the aging a tail develops in transients measured at t_i and $t_i + 2000$ s.

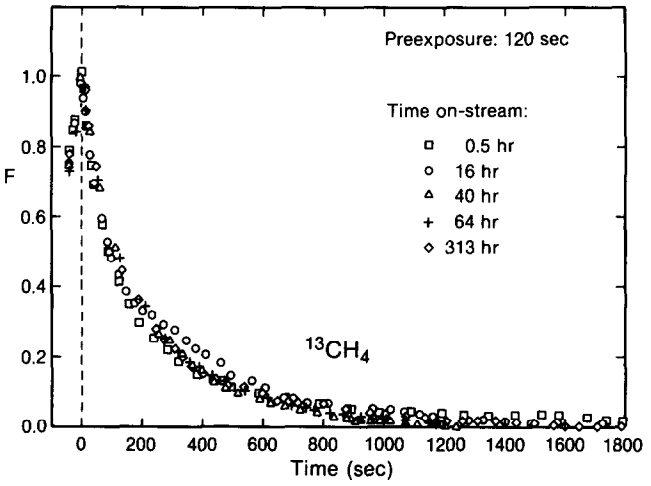

FIG. 8. The transients measured at $t_i = t_i + 4120$ s, unlike those measured at t_i and $t_i + 2000$ s, *do not* change upon aging.

are missing in the transients measured at $t = t_i + 4120$ s. This puts certain demands on the reaction pathway(s).

Consider first a pathway covering the catalyst with only *one* type of intermediate, I^-*:

$$A(g) \rightarrow I^-* \rightarrow B(g) \qquad (2)$$

Assume that A, I^-*, and B all contain one carbon atom only. Further definitions necessary for a treatment of the isotope transients are

$N_{12}(N_{13})$: the number of surface intermediates I_{12} (i.e., containing a carbon atom ^{12}C) (moles);

$F_{12} = \dfrac{N_{12}}{N_{12} + N_{13}}$, with $F_{12}(F_{13})$ being the fractional isotopic composition of the pool of N surface intermediates, I^-*;

R: the reaction rate (moles).

A(g) in this treatment is to be identified with CO(g), B(g) with CH_4, and I^-* with a carbon-derived surface species. If we assume that prior to $t = 0$ the system is under $^{13}CO/H_2$ for a long time, then

$$F_{13} = 1; \quad F_{12} = 0 \qquad (3)$$

$$N_{13} = N; N_{12} = 0. \qquad (4)$$

At $t = 0$ we switch from $^{13}CO/H_2$ to $^{12}CO/H_2$ and for $t > 0$ we have

$$\frac{dN_{13}}{dt} = -RF_{13} \qquad (5)$$

with

$$dN_{13} = d(N \cdot F_{13}) = NdF_{13}. \qquad (6)$$

We obtain

$$\frac{dF_{13}}{dt} = -\frac{1}{(R/N)} F_{13} = -\frac{1}{\tau} F_{13}. \qquad (7)$$

R, N, and τ in (7) all are F_{13}-independent quantities. As ^{12}CO and ^{13}CO have virtually identical chemical properties the change from $^{13}CO/H_2$ to $^{12}CO/H_2$ does not produce any change in reaction rate. Accordingly, (7) integrates into

$$F_{13} = (F_{13})_{t=0} e^{-\frac{t}{\tau}} = e^{-\frac{t}{\tau}}. \qquad (8)$$

According to Eq. (8) the ^{13}C content of a single homogeneous pool/reservoir of intermediates will, in $^{12}CO/H_2$ atmosphere, decrease exponentially. The rate of decrease will be faster for a smaller pool size (N) and a larger exit stream (R):

$$\tau = \frac{N}{R} \text{ (s)}. \qquad (9)$$

Therefore, the relaxation constant τ is a characteristic property of the pool/reservoir of intermediates. A single homoge-

neous pool (CSTR) relaxes with a single relaxation constant, τ.

We now consider transients from partially exchanged systems, such as those starting at point 3 in Fig. 4. Consider the system to be sufficiently long under $^{12}CO/H_2$ as characterized by $F_{13} = 0$ ($t = 0$). At $t = 0$ we switch from $^{12}CO/H_2$ to $^{13}CO/H_2$, and at $t = \Delta t$ we switch back to $^{12}CO/H_2$ (cf. to Fig. 4; $t = 0$ corresponds to $t = t_i + 4000$ s in Fig. 4: $t = \Delta t$ corresponds to $t = t_i + 4120$ s in Fig. 4). We have

$$F_{13} = 0 \quad (t = 0) \tag{10}$$

$$F_{13} = 1 - e^{-\frac{t}{\tau}} \quad (0 \le t \le \Delta t) \tag{11}$$

$$F_{13} = 1 - e^{-\frac{\Delta t}{\tau}} \quad (t = \Delta t) \tag{12}$$

and

$$F_{13} = (1 - e^{-\frac{\Delta t}{\tau}})e^{-\frac{(t-\Delta t)}{\tau}} \quad (t \ge \Delta t). \tag{13}$$

From a comparison of (13) with (8) it follows that both a partially and completely exchanged pool relax with a single relaxation constant, τ. After normalization the partially and fully exchanged case become indistinguishable. Experimentally, however, the partially exchanged case (Fig. 6) is distinguishable from the more fully exchanged case (Fig. 5). This leads us to a conclusion (*3*) that we are witnessing the combined behavior of at least *two* pools of surface intermediates.

Figure 9A gives one of several possible two-pool models: two pools in *series*. Below we prove that this configuration cannot be responsible for the difference between transients (1) and (2), at the one hand (Fig. 5), and transient (3) at the other (Fig. 6). We start with both pools filled with ^{12}C. Upon exposure to $^{13}CO/H_2$ ($t \ge 0$) we obtain for pool 1 (^1F):

$$^1F_{13} = 1 - e^{-\frac{t}{\tau_1}}. \tag{14}$$

In a unidirectional pathway the behavior of pool 1 is independent of that of pool 2, and (14) therefore is identical to (11). $^1F_{13}$ acts as the input function for the second pool. A mass balance on pool 2 leads to (cf. Appendix)

$$^2F_{13}(t) = 1 - \frac{\tau_1}{\tau_1 - \tau_2} e^{-\frac{t}{\tau_1}} + \frac{\tau_2}{\tau_1 - \tau_2} e^{-\frac{t}{\tau_2}}. \tag{15}$$

Two features are noteworthy, i.e.,

$$^1F_{13}(t) > {}^2F_{13}(t) \tag{16}$$

and

$$\left(\frac{d^2F_{13}}{dt}\right)_{t=0} = 0. \tag{17}$$

The features (16) and (17) arise essentially from the same effect: pool 1 delays the entrance of ^{13}C into pool 2.

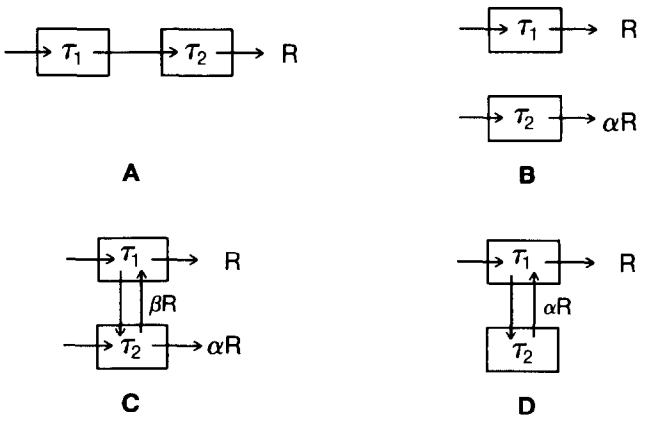

FIG. 9. Different configurations of two pools of intermediates.

If we leave the system for a time Δt in contact with $^{13}CO/H_2$, and then switch back to $^{12}CO/H_2$, the partially exchanged pools will relax as ($t \geq \Delta t$)

$$^1F_{13} = (1 - e^{-\frac{\Delta t}{\tau_1}})e^{-\left(\frac{t-\Delta t}{\tau_1}\right)} \quad (18a)$$

and

$$^2F_{13} = \frac{\tau_1}{\tau_1 - \tau_2} e^{-\left(\frac{t-\Delta t}{\tau_1}\right)} - \frac{[(\tau_2 e^{-\frac{\Delta t}{\tau_2}} + \tau_1(1 - e^{-\left(\frac{-\Delta t}{\tau_1}\right)})]e^{-\left(\frac{t-\Delta t}{\tau_2}\right)}}{\tau_1 - \tau_2}. \quad (18b)$$

It emerges that

$$\left(\frac{d^2F_{13}}{dt}\right)_{t=\Delta t} > 0, \quad (19)$$

i.e., in $^{12}CO/H_2$ atmosphere the ^{13}C content of pool 2 initially increases before it decreases. In essence, this is the consequence of the fact that ^{13}C ex-^{13}CO penetrates into pool 1 *before* it penetrates into pool 2. This leads to Eq. (16), and therefore to (19).

In the actual experiments we observe (cf. Fig. 6)

$$\left(\frac{d^2F_{13}}{dt}\right)_{t=t_i+4120\,s} < 0. \quad (20)$$

This leads us to reject the proposition that the difference between the partially and more fully relaxed transients derive from the effect of two or more pools *in series*. We conclude that the observed effects derived from two or more pools *in parallel*.

For two independent reservoirs (Fig. 9B) the combined relaxation is merely the sum of that of the two constituents:

$$^{13}F_t = \frac{1}{1 + \alpha} e^{-\frac{t}{\tau_1}} + \frac{\alpha}{1 + \alpha} e^{-\frac{t}{\tau_2}} \quad (21)$$

in which F_t is the isotopic composition of the completely mixed exit streams of the two pools. For $\tau_2 \gg \tau_1$ an exponential decay with a "tail" originates (*16*), similar to the responses observed at $t = t_i$ and $t = t_i + 2000$ s (Fig. 7).

In order to find the behavior of a partially exchanged system of two parallel reservoirs we start with both systems containing ^{12}C exclusively ($t = 0$). After exposure to $^{13}CO/H_2$ for a period Δt we have

$$^{13}F_1 = 1 - e^{-\frac{\Delta t}{\tau_1}} \quad (22)$$

and

$$^{13}F_2 = 1 - e^{-\frac{\Delta t}{\tau_2}}. \quad (23)$$

Switching back to $^{12}CO/H_2$ at $t \geq \Delta t$ leads to

$$^{13}F_t = N[((1 - e)^{-\frac{\Delta t}{\tau_1}}) \frac{1}{1 + \alpha} e^{-\frac{t-\Delta t}{\tau_1}} + (1 - e^{-\frac{\Delta t}{\tau_2}}) \frac{\alpha}{1 + \alpha} e^{-\frac{t-\Delta t}{\tau_2}}] \quad (24)$$

with N a normalization factor.

It follows that an exposure $\Delta t \ll \tau_2$ leads to a suppression of the component $\exp(-(t - \Delta t)/\tau_2)$ in the subsequent relaxation. What happens for a sequence $^{12}CO/H_2 \rightarrow {}^{13}CO/H_2(\Delta t) \rightarrow {}^{12}CO/H_2$ is that the slowly relaxing reservoir does not fill appreciably with ^{13}C in the period Δt. Therefore it does not produce a pronounced amount of ^{13}C in the subsequent $^{12}CO/H_2$ stage: the "tail" is absent. This is what we observed experimentally (Fig. 8).

In order to verify the above we measured after 2 weeks on stream a series of transients in $^{12}CO/H_2$, obtained after exposing the catalyst to $^{13}CO/H_2$ for a period Δt which varied between 120 and 1800 s. From the responses (Fig. 10), it emerges that the $\tau \approx 1000$ s component (the "tail") in the relaxation pattern increases with increasing exposure, Δt. This result confirms that we are working with reservoirs positioned in parallel rather than in series.

The other "two-reservoirs-in-parallel" models (Figs. 9C,D) give analytical solutions:

$$F = Ae^{-\frac{t}{\tau_\alpha}} + (1 - A)e^{-\frac{t}{\tau_\beta}} \quad (25)$$

which are indistinguishable from the solution given in Eq. (15) for model 9B (cf. Appendix). As the time (t) and frequency ($1/\Delta t$) responses are related to a one-to-one

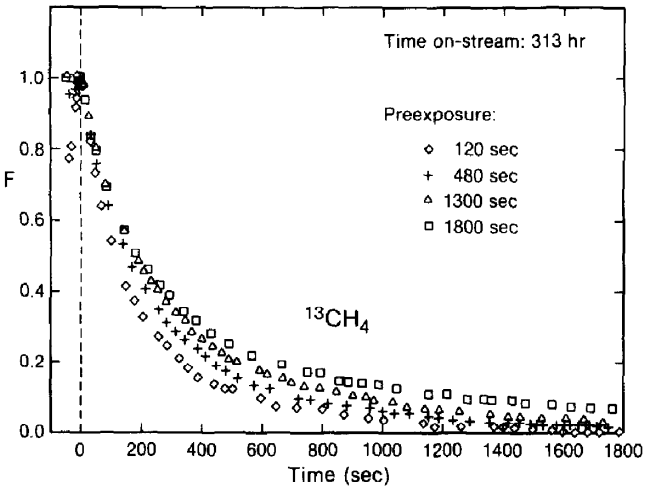

FIG. 10. The decay of $^{13}CH_4$ varies with the time of preexposure (Δt) to $^{13}CO/H_2$.

manner these models also cannot be distinguished by looking for variation in relaxation with varying exposure, i.e., by experiments of the type depicted in Fig. 10. However, what models 9B–D all share is that at least for part of the pathway from CO to CH_4, there are two parallel, independent routes. We will focus on this feature, and what it means in terms of processes underlying aging. In doing so we confine ourselves to model 9B with its simple relations (cf. Eq. (25) with Eq. (15) and Fig. 9B):

$$\tau_\alpha = \tau_1 \tag{26a}$$

$$\tau_\beta = \tau_2 \tag{26b}$$

$$A = \frac{1}{1 + \alpha}. \tag{26c}$$

Our conclusion, however, will also be valid whenever Figs. 9C,D rather than Fig. 9B describes the actual system.

The preceding analysis of the relaxation of partially exchanged systems indicates the following.

(1) We are dealing with at least two pools of intermediates.

(2) These pools are positioned (partially) in parallel rather than in a series.

(3) Such a parallel configuration leads to a relaxation curve consisting of a sum of two exponentials.

(4) The relative contribution of the component with the shorter time constant can be accentuated by measuring the relaxation after short exchange times.

It follows that we should determine τ_1 (with, by definition, $\tau_1 < \tau_2$) from the transients starting at $t = t_i + 4120$ s (cf. Fig. 4). These transients are given in Fig. 8. From inspection of Fig. 8 it emerges, and this is one of the main findings in the present study, that τ_1 is highly independent of catalyst aging.

An unweighed least-square fit of Fig. 8 to

$$F(t) = (A - B)e^{-\frac{t}{\tau_1}} + B \tag{27}$$

yields

$$\tau_1 = 120 \pm 20 \text{ s}$$

and

$$B = 0.05 \pm 0.1$$

with the values quoted as $\pm$ being single standard deviations. Component B has been included to account for both unresolved low-frequency components and uncertainty in separation of the signal from the background.

With the value $\tau_1 = 120$ s obtained from the transients measured at $t = t_i + 4120$ s, we deconvoluted the transients measured at $t = t_i$ and $t = t_i + 2000$ s into

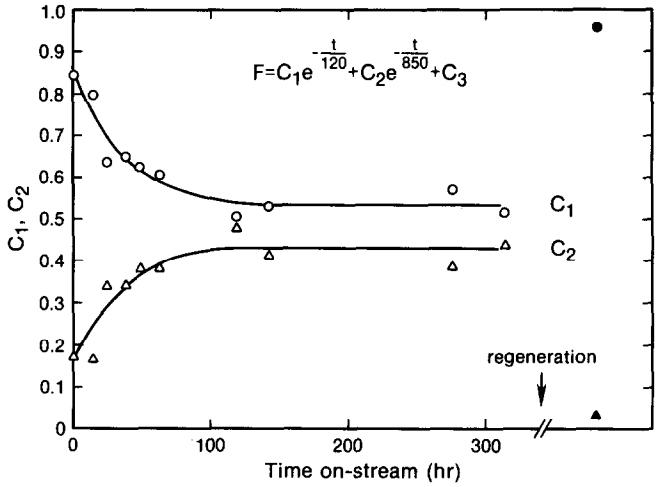

FIG. 11. Variation with line out of the relative contribution of the $\tau_1 = 120$ s and $\tau_2 = 850$ s component to the total CH_4 make.

$$F(t) = (A - B)e^{-\frac{t}{120}} + (1 - A - B)e^{-\frac{t}{\tau_2}} + B. \quad (28)$$

No trend of τ_2 with time on stream is discernible, and we obtain

$$\tau_2 = 850 \pm 200 \text{ s}.$$

What is changing with time-on-stream, however, are the relative contributions to the total methane production of the 120- and 850-s reservoir. Figure 11 gives the amplitudes of the 120- and 850-s components (Eq. (28)) as a function of time on stream. The 850 s component (the "tail") increases at the expense of the 120 s component, and lining out takes place parallel with that of the activity (compare Fig. 11 with Fig. 1). It is apparent that the initial decrease in TOF and the development of a reservoir of intermediates with reactivity $k \approx 1/850$ s are manifestations of the same lining out phenomenon.[2]

In the introduction we considered as a possible cause of the lining out phenomenon the building up of less reactive carbon, CH_y, balanced after approximately 120 h by the removal reaction (k_2)

$$\begin{array}{ccccccc} CO(g) & \xrightarrow{k_a} & CH_x\text{-soft} & \xrightarrow{k_b} & CH_y\text{-hard} & \xrightarrow{k_c} & C_{graphite} \\ & & \downarrow k_1 & & \downarrow k_2 & & \\ & & CH_4(g) & & CH_4(g) & & \end{array} \quad (A)$$

Because of what has been inferred about reservoirs in series versus reservoirs in parallel (Fig. 9) we have to consider alternatives such as

$$\begin{array}{ccccc} & \overset{k_a}{\nearrow} & CH_x\text{-soft} & \xrightarrow{k_1} & CH_4(g) \\ CO(g) & & (\Updownarrow) & & \\ & \underset{k_b}{\searrow} & CH_y\text{-hard} & \xrightarrow{k_2} & CH_4(g) \end{array} \quad (B)$$

or

$$\begin{array}{ccccc} CO(g) & \xrightarrow{k_a} & CH_x\text{-soft} & \xrightarrow{k_1} & CH_4(g) \\ & & k_2 \Updownarrow k_{-2} & & \\ & & CH_y\text{-hard} & & \end{array} \quad (C)$$

These and similar schemes share that CH_y-hard gradually builds up, and that lining out is caused by a CH_y-removal reaction balancing the CH_y-formation reaction. Lining out occurs at an interval of the order of 120 h (Fig. 1). This implies that the formation/removal reaction equilibrates in about 120 h, *and further that CH_y-hard itself has a lifetime τ of about 120 h*. However, the

[2] We mention that deconvolution of the tailing transients with *both* τ_1 and τ_2 as fitting parameters leads to considerably more noise than the procedure followed at present, i.e., changing the preexposure time and inferring τ_1 from the transients of the partially exchanged system.

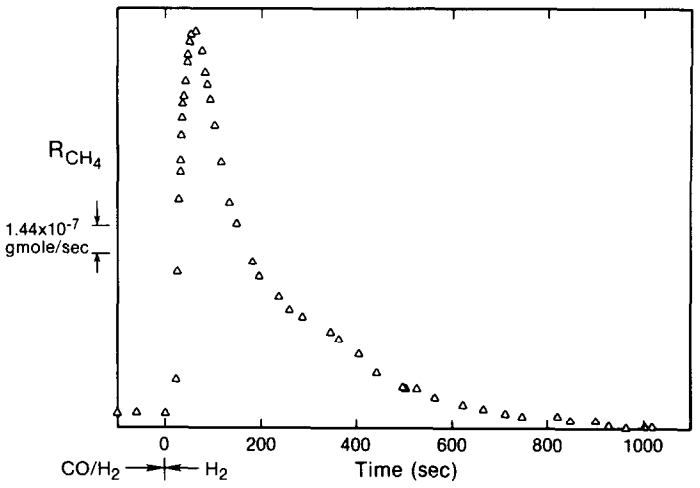

FIG. 12. Methane production in pure H_2 signals a large reservoir of (dissolved) carbon.

transient experiments demonstrate CH_y-hard to have a lifetime of the order of 850 s. This rules out all schemes such as A–C, that feature buildup of CH_y-hard as the cause of the lining out.

Now we consider surface blocking by a third type of carbon, say $C_{graphite}$, exhibiting a $\tau \approx 120$ h. The contribution of such carbon to the transients will vanish in the background. Actually, there is ample evidence for a large pool of additional carbon (see below). However, this pool apparently does not block the surface. We infer this from the following observations.

- The total CO_{ad} uptake increases with time on stream (Fig. 3).
- The combined coverage $\theta_{CH_x} + \theta_{CH_y}$ increases with time on stream, excluding surface blocking to underlie the lining out.

Above, we eliminated a change in the reactive and a change in the irreactive (i.e., merely surface blocking) overlayer as primary causes of the line out phenomenon. *Therefore, we conclude that rather than a change in the adlayer, the line out reflects a slow change in the catalytic properties of the "nickel" itself.*

We reached the previous conclusion without making mechanistic assumptions or drawing on any evidence but that provided by the transients. However, we cannot proceed much beyond this point. We subjected the aged catalyst at reaction temperature to an exposure in pure hydrogen. The following findings are evident.

(1) A carbon reservoir of over 10 monolayer *equivalents* appears (Fig. 12).

(2) The size of the reservoir (i.e., N), together with the rate of removal R in CO/H_2 atmosphere (an upper limit can be calculated from the background in the transients) signals carbon with a long lifetime:

$$\tau = \frac{N}{R} \geq 10 \text{ h}.$$

(3) The carbon removal restores the original shape of the transients (Fig. 11).

(4) The regenerated catalyst has a methanation activity and capacity for CO uptake slightly above that of the fresh catalyst (Figs. 1 and 3, respectively), and a TOF which is almost identical to that of the fresh catalyst.

Finding (1) indicates "dissolution" into the Raney nickel of significant amounts of carbon. Consistency with the transient-kinetic observations arises when we assume that on a 120-h time scale the carbon uptake proceeds to completion for one part of the specimen, whereas the other part remains essentially free of carbon. The 120- and 850-s transients then reflect catalysis over,

respectively, the "clean" and carbon-containing Raney nickel. The implied heterogeneity of the fresh sample could derive from bimodality in either the crystallite size, morphology, or aluminum content.

APPENDIX

Mathematical Models

Model A (Fig. 9):

$$F = \frac{\tau_1}{\tau_1 - \tau_2} \exp\left(\frac{-t}{\tau_1}\right) - \frac{\tau_2}{\tau_1 - \tau_2} \exp\left(\frac{-t}{\tau_2}\right)$$

Model B (Fig. 9):

$$F = \frac{1}{\alpha + 1} \exp\left(\frac{-t}{\tau_1}\right) + \frac{\alpha}{\alpha + 1} \exp\left(\frac{-t}{\tau_2}\right)$$

Model C (Fig. 9):

$$F = A \exp\left(\frac{-t}{\tau_\alpha}\right) + (1 - A)\exp\left(\frac{-t}{\tau_\beta}\right)$$

$$A = \frac{1}{(\alpha + 1)}\left(1 + \alpha + \frac{\alpha}{\beta} - \frac{\tau_1\alpha}{\tau_\alpha\beta}\right)\frac{\left(1 - \frac{\tau_1}{\tau_\beta}\right)}{\tau_1\left(\frac{1}{\tau_\alpha} - \frac{1}{\tau_\beta}\right)}$$

$$\tau_\alpha, \tau_\beta = \frac{1}{\left[\frac{1}{2\tau_2}\left(1 + \frac{\beta}{\alpha}\right) + \frac{1}{2\tau_1}(1 + \beta)\right.}$$

$$\left. \mp \sqrt{\left(\frac{1}{2\tau_2}\left(1 + \frac{\beta}{\alpha}\right)\right)^2 + \left(\frac{1 + \beta}{2\tau_1}\right)^2 + \frac{(1 + \beta)(1 + \beta/\alpha)}{2\tau_1\tau_2} - \frac{(1 + \beta + \beta/\alpha)}{\tau_1\tau_2}}\right]$$

Model D (Fig. 9):

$$F = A \exp\left(\frac{-t}{\tau_\alpha}\right) + (1 - A)\exp\left(\frac{-t}{\tau_\beta}\right)$$

$$A = \frac{\left(1 - \frac{\tau_1}{\tau_\beta}\right)}{\tau_1\left(\frac{1}{\tau_\alpha} - \frac{1}{\tau_\beta}\right)}$$

$$\tau_\alpha, \tau_\beta = \frac{1}{\left[\frac{1}{2\tau_1} + \frac{1}{2\tau_2} + \frac{\alpha}{2\tau_1} \mp \sqrt{\left(\frac{1}{2}\left(\frac{1}{\tau_1} + \frac{1}{\tau_2} + \frac{\alpha}{\tau_1}\right)\right)^2 - \frac{1}{\tau_1\tau_2}}\right]}$$

ACKNOWLEDGMENTS

We gratefully acknowledge support of this work by the U.S. Department of Energy, Office of Basic Energy Sciences (Contract DE-AC02-83ER13105) and by the Exxon Education Foundation.

REFERENCES

1. Beeck, O., *Rev. Mod. Phys.* **17,** 61 (1945).
2. Boudart, M. "Kinetics of Chemical Processes." Prentice–Hall, New York, 1968.
3. Biloen, P., Helle, J. N., van den Berg, F. G. A., and Sachtler, W. M. H., *J. Catal.* **81,** 450 (1983).
4. Dautzenberg, F. M., Helle, J. N., Biloen, P., and Sachtler, W. M. H., *J. Catal.* **63,** 119 (1980).
5. Wentrcek, P. R., Wood, B. J., and Wise, H., *J. Catal.* **43,** 363 (1976).
6. Araki, J. M., and Ponec, V., *J. Catal.* **44,** 439 (1976).
7. Biloen, P., Helle, J. N., and Sachtler, W. M. H., *J. Catal.* **58,** 95 (1979).
8. Bonzel, H. P., and Krebs, H. J., *Surf. Sci.* **91,** 499 (1980).
9. McCarty, J. G., and Wide, H., *J. Catal.* **57,** 406 (1979).
10. Goodman, D. W., Kelley, R. D., Madey, T. E., and White, J. M., *J. Catal.* **64,** 479 (1980).
11. Bell, A. T., Winslow, P., *in* "Proceedings, 8th International Congress on Catalysis, Berlin, 1984," Vol. III, p. 175.
12. Freel, J., Robertson, S. D., and Anderson, R. B., *J. Catal.* **18,** 243 (1970).
13. Yang, C.-H., Soong, Y., and Biloen, P., *in* "Proceedings, 8th International Congress Catalysis, Berlin, 1984," Vol. II, p. 3.
14. Happel, J., Suzuki, J., Kokayeff, P., and Fthenakis, V., *J. Catal.* **65,** 59 (1980).
15. Dr. D. G. Blackmond's chemisorption measurements are gratefully acknowledged.
16. Otarod, M., Osawa, S., Yin, F., Chew, M., Cheh, H. Y., and Happel, J., *J. Catal.* **84,** 156 (1983).